

Site-specific Quantification of Bone Quality using Highly Nonlinear Solitary Waves

J. Yang^a, S. Sangiorgio^b, S. Borkowski^b, C. Silvestro^c,
L. De Nardo^c, C. Daraio^a and E. Ebrahimzadeh^b

^a*Graduate Aeronautical Laboratories (GALCIT)
California Institute of Technology, Pasadena, California 91125*

^b*J. Vernon Luck, MD Orthopaedic Research Center
Los Angeles Orthopaedic Hospital, Los Angeles, California 90007*

^c*Dipartimento di Chimica, Materiali e Ingegneria Chimica "G. Natta"
Politecnico di Milano, Milano 20133, Italia*

ABSTRACT

Osteoporosis is a well recognized problem affecting millions of individuals worldwide. Consequently, the need to effectively, efficiently, and affordably diagnose and identify those at risk is essential; moreover, site-specific assessment of bone quality is necessary, not only in the process of risk assessment, but may also be desirable for other applications. The present study evaluated a new one-dimensional granular crystal sensor, composed of a tightly packed chain of beads under Hertzian contact interaction, representing the most suitable fundamental component for solitary wave generation and propagation. First, the sensitivity of the novel sensor was tested using densities of rigid polyurethane foam, representing clinical bone quality ranging from healthy, to severely osteoporotic. Once the relationship between the signal response and known densities was established, the sensor was used to measure several sites located in the proximal femur of ten human cadaveric specimens. The accuracy of the model was then further investigated, using measurements of bone quality from the same cadaveric specimens, independently, using DEXA. The results indicate not only that the novel technique is capable of detecting differences in bone quality, but that the ability to measure site-specific properties without exposure to radiation, has the potential to be further developed for clinical applications.

I. INTRODUCTION

Worldwide, osteoporosis affects hundreds of millions of people. In the United States alone, more than 10 million individuals over the age of 50 are known to have osteoporosis. Further, according to the Surgeon General, osteoporosis is responsible for an estimated 1.5 million fractures a year. In elderly patients, hip fractures are often treated by performing a total hip replacement (arthroplasty) operation, which are known to have better outcome in patients with better bone quality [1]. With the frequency of total joint surgeries expected to drastically increase over the next decades, which in turn will lead to an adverse effect on hospital costs, surgeon availability and healthcare expenses, the ability to accurately diagnose and treat patients with osteoporosis would be beneficial [2-3].

Currently, the tools that are available for bone quality assessment include dual energy X-ray absorptiometry (DEXA), quantitative computerized tomography (qCT), and quantitative ultrasound (QUS). Each of these technologies provides unique information, yet none offer comprehensive, site-specific evaluation of bone mechanical properties in a noninvasive and time-efficient manner. For example, DEXA is routinely used to screen for osteoporosis and osteopenia; however, it is a two-dimensional quantification which averages bone mineral density (BMD) over relatively large geometric regions of interest. In addition to the lack of a direct measurement of

bone quality and its relation to fracture, the DEXA scan also requires a large machine, multiple x-rays, and a scored analysis performed by a radiologist [4].

Discrepancies concerning how each method relates to fracture risk exist throughout the literature. Kanis et al showed that BMD was correlated to fracture strength, but that certain additional parameters need to be considered to predict fracture risk [5]. Lochmuller et al. compared the use of DEXA, pQCT, and QUS in determining the likelihood of fracture of the femur, spine, and radius, concluding that DEXA most accurately assessed femoral strength, while all three methodologies were comparable for the spine and radius [6]. Stewart et al. compared the use of DEXA and QUS in menopausal woman, reporting that while typically less expensive, QUS was a better predictor of fracture [7].

In the laboratory, Myers et al. correlated the fracture strength to BMD in a cadaveric forearm model. They reported that geometric analysis from the DEXA scans was a better predictor of fracture than bone mineral density [8]. Roberts et al. evaluated the correlation between absolute BMD and stiffness derived from load-displacement tests using sideways-fall simulation, concluding that absolute BMD thresholds were well above the clinically tolerable threshold. Based on these findings, they suggested that a mechanical determination of fracture strength should be utilized instead of relying solely on bone mineral density scans [9].

Although DEXA scans are currently accepted in the clinical arena as standalone determinant of bone quality, this is an oversimplification of a very complex mechanical phenomenon. Specifically, bone is anisotropic and nonhomogeneous, and its strength in any given direction is influenced by not only BMD, but by the complex microstructural orientation of the organic collagen matrix in which the mineral portion is embedded.

This study introduces and evaluates a novel method for nondestructive site-specific evaluation (NDSE) of bone mechanical properties. Highly nonlinear solitary waves (HNSWs) are used to investigate bone mechanical properties based on their interaction with bone at a specific location. The HNSWs are compactly-supported lumps of energy, which are generated by a balance of nonlinear and dispersive effects in intrinsically nonlinear media, such as granular and layered materials [10-11]. Leveraging recent theoretical and numerical elucidation on the HNSW propagation principles and the advent of artificially fabricated meta-materials, solitary waves are expanding their applications to, for example, shock and impact/sound absorbing layers [12-13], acoustic lens devices [14], and diagnostic scanning device [15].

The present study evaluated a new one-dimensional granular crystal sensor, composed of a tightly packed chain of beads, governed by Hertzian contact laws, which represents the most suitable fundamental component for solitary wave generation and propagation [10, 16]. The granular crystal sensor transmits a single pulse of HNSW into the biological system via direct contact, and record its responses in the form of disintegrated solitary wave packets reflected from the interface. Previous studies have shown that the scattering of solitary waves at the granular crystal interface is significantly affected by the mechanical properties of bounding medium. This is a unique wave dynamics and energy localization phenomenon that has never been observed in the linear medium [17-18]. Experimental measurements of the propagation of HNSWs are determined with respect to a range of both artificial and cadaveric bone samples, exploiting the responsiveness of HNSWs to adjoined media. Using a numerical tool based on highly nonlinear dynamics, bone quality is assessed based on the coupling behavior between the granular crystal and bone microstructure. The aim of the study was to evaluate the accuracy and precision of the solitary wave-based method for site-specific measurement of bone quality. In particular, we hypothesize that compared to overall proximal femur BMD measurement as determined by DEXA, a stronger correlation would be found between site-specific BMD measurement and solitary wave output. If successfully validated, the proposed solitary wave-based evaluation method has the potential to become a quick and reliable method for site-specific assessment of bone quality.

II. MATERIALS AND METHOD

A. HNSW-based Evaluation Method

Experimental setup

A one-dimensional granular crystal was assembled using 20 stainless steel beads to form a sensor device prototype (McMaster-Carr, Elmhurst, Illinois, type 440C, Young's modulus $E = 200$ GPa, density $\rho = 7780$ kg/m³, Poisson's ratio $\nu = 0.27$, radius $R = 9.525$ mm) (Fig. 1). A single pulse of solitary waves was generated by impacting the chain of beads with an identical striker. The striker was released from a drop height of 5-mm using a DC-powered linear solenoid to generate a single pulse of the HNSW [18]. The temporal profiles of both the incident and reflected solitary waves were recorded using an instrumented bead embedded with calibrated piezoceramics [16]. In this study, the instrumented bead was positioned at the 14th position from the interface (i.e., 7th bead from the top of the chain, excluding the striker). The force histories measured by the instrumented particle were acquired using an NI data acquisition card (PCI-6115, National Instruments, Austin, Texas), which was connected to a computer for digital signal processing.

Numerical setup

A discrete particle model [10, 18] was used to numerically evaluate the responses of the HNSWs for a range of bone specimens. In this model, the particle dynamics in the monodispersed granular chain is described by the interaction of lumped masses and nonlinear springs [Fig. 2]. The forces between neighboring particles are regulated by Hertzian contact law expressed as $F \propto \delta^{3/2}$, where F is force and δ is approach between particles. The equation of motion of such a nonlinear spring-type spherical lattice can be expressed as:

$$m\ddot{u}_n = A_n[u_{n-1} - u_n]_+^{3/2} - A_{n+1}[u_n - u_{n+1}]_+^{3/2} + f, \quad n \in \{1, \dots, N\},$$

$$A_n \equiv \begin{cases} A|_c = \frac{E\sqrt{2R}}{3(1-\nu^2)} & n \in \{1, \dots, N\} \\ A|_w = \frac{4\sqrt{R}}{3} \left(\frac{1-\nu^2}{E} + \frac{1-\nu_w^2}{E_w} \right)^{-1} & n = N+1 \end{cases} \quad (1)$$

Here m is the mass of the bead, u_n is the displacement of the given particle from its equilibrium position, and f is the body force applied to the bead – gravity in this study. The bracket $[s]_+$ takes only positive values and returns 0 if $s < 0$. This means that the discrete particle model for the tightly-packed granular chain is dictated by the double nonlinearity: a nonlinear force under compression and a zero tensile force [19]. The coefficient of the nonlinear spring in the chain $A|_c$ is a function of E , ν , and R , which are Young's modulus, Poisson's ratio, and the radius of the granular element. On the other hand, the nonlinear spring coefficient $A|_w$ at the end of the chain is governed by the material properties of the bone denoted by subscript w , as well as the bead material properties.

Ordinary differential solvers in MATLAB were used to numerically integrate Eq. (1) for the simulation of the HNSW interactions with bone materials over a range of mechanical properties [20]. As a result, a single packet of robust HNSW (blue curve in Fig. 1 with the shape of cosine to the fourth mathematically) is generated. After its collision with the wall, the incident solitary wave is disintegrated into a series of solitary waves (red curve). This unique physical phenomenon is caused by the acoustic wave localization at the interface between different physical media, specifically in this study, the nonlinear granular chain and the bone structure [18].

The effect of bone mechanical properties on the backscattering and postponement of the reflected solitary waves was investigated. In particular, the time of flight (TOF), which represents the time elapsed between the incident and the reflected solitary waves, was evaluated to describe

its correlation to the bone material properties. Among a train of reflected solitary waves, the first reflected solitary waves (herein referred to as primary solitary waves) were used to extract the information about the bone mechanical properties. The relationship between the TOF and Young's modulus obtained from numerical simulations is used to interpolate the experimentally measured TOF to derive a calculated Young's modulus of bone specimens.

Validation using synthetic bone with known material properties

Preliminary testing was performed to establish the sensitivity of the HNSWs to the mechanical properties of neighboring media, using artificial bone materials with clinically relevant material properties. Seven different densities of rigid polyurethane foam (Pacific Research Laboratories, Inc., Vashon, Washington) were tested to simulate clinical bone quality ranging from healthy, to severely osteoporotic [21-22]. (Table 1) Each artificial cancellous bone sample was cut into a 50×50×50 mm block, and five measurements of reflected HNSWs were obtained for each sample.

Table 1

Specifications of artificial cancellous bone samples made of polyurethane foam [21].

Sample	Density [g/cc]	Compressive strength [MPa]	Young's modulus [MPa]	Osteoporotic categorization [23-24]
1	0.08	1.0	32	High risk of fracture
2	0.16	2.2	58	Osteoporotic
3	0.24	4.9	123	Healthy
4	0.32	8.4	210	Healthy
5	0.48	18	445	Healthy
6	0.64	31	759	Healthy
7	0.80	48	1148	Healthy

B. Evaluation of Proximal Femoral Bone Quality

Specimen preparation

Ten fresh-frozen human cadaveric femurs were selected to represent a range of quality and sizes. High-resolution anteroposterior (AP) and mediolateral (ML) radiographs were taken of each specimen using an HP Faxitron Series™ x-ray system (43805N, Hewlett Packard Company, Palo Alto, California) at the standard 15% clinical magnification. Radiographic analysis of each specimen was performed prior to experimentation to determine bone health. Additionally, the radiographs were examined for signs of evident bone disease, injury, or abnormalities. Excess soft tissue was carefully removed in the proximal region of the femur to expose the cortical surface of each specimen while preserving the bony surface. All specimens were kept frozen before and after testing, and thawed to room temperature immediately prior to HNSW evaluation.

DEXA Analysis

The bone mineral density (BMD) of all ten specimens was assessed by dual-energy x-ray absorptiometry (DEXA) using a Hologic 2000 bone densitometer (Hologic, Inc., Waltham, MA) and a soft tissue substitute, to mimic patient conditions. For each specimen, the standard clinical regions were measured and calculated: (1) femoral neck, (2) trochanteric region, (3) inter trochanteric region, (4) Ward's area, and (5) proximal femur. For each scan, area (cm²), bone mineral content (BMC) (g), and BMD (g/cm²) were recorded.

Cadaveric HNSW Measurements

Using the identical apparatus that was used to measure the synthetic bone specimens, site-specific nondestructive evaluation was conducted for each cadaveric femur. For each specimen, the HNSW-based evaluation was done at 12 locations: anterior femoral neck, posterior femoral neck, superior greater trochanter, lateral greater trochanter, anterior greater trochanter, posterior greater trochanter, anterior inter trochanteric region, posterior inter trochanteric region,

superior femoral head, medial femoral head, anterior femoral head, and posterior femoral head (Fig. 3). For each location, five repetitive tests were performed to acquire the mean time of flight information of primary reflected solitary waves. They were interpolated to extract the corresponding Young's modulus of bone specimens based on the numerical relationship between bone Young's modulus and time of flight.

C. Statistical Analysis

The categorical input variables for this study were BMD measurement areas (five scanning areas of DEXA testing) and HNSW recording location (twelve testing locations of site-specific HNSW-based evaluation). The primary outcome variables were 1) BMD, 2) primary solitary waves' time of flight, and 3) derived Young's modulus. Statistical analysis was done to determine the strength of correlation between the BMD measurements and the HNSW measurements. SPSS 15.0 statistical analysis software (SPSS, Inc., Chicago, IL) was used to assess the bivariate pearson correlation between 1) proximal femur BMD (non site-specific) and HNSW time of flight/Young's modulus and 2) site-specific BMD and HNSW time of flight/Young's modulus. Pearson correlation (r) values were determined, each with an associated p-value. Linear regression analysis was used to determine the strength of each correlation, represented by the slope of each regression.

III. RESULTS

A. Preliminary validation using synthetic bone with known material properties

Propagation of the HNSWs in a temporal domain was successfully recorded and numerically simulated for the interactions with the various rigid polyurethane foams (Fig. 4). The first packet of propagating waves corresponds to the incident solitary wave passing by the 7th bead in the chain. When comparing experimentally and numerically generated waveforms, approximately identical incident waves were formed and propagated in each case. The subsequent impulses represent the solitary waves reflected at the interface of the rigid polyurethane foam specimens. The reflected wave profiles show clear differences between the various samples. In particular, the interaction with the more "osteoporotic" specimens results in further delay in the arrival of the reflected solitary waves to the instrumented sensor, compared to that of the more "healthy" specimens.

The delay time of the primary solitary waves is extracted from the experimental and numerical signals in terms of the TOF, and they are plotted as a function of Young's modulus (Fig. 5). The TOF of the primary solitary waves exhibit strong dependence on the Young's modulus of bone. According to the experimental results, the TOF in the "osteoporotic" sample (Spl-2) is increased by 61.4%, from 1.32 ms to 2.13 ms, in comparison to the most healthy sample (Spl-7). Further postponement of primary reflected solitary waves' arrival (2.49 ms) is obtained if the bone quality is degraded to the "high risk of fracture" level (Spl-1).

The simulation results based on the discrete particle model in Section II closely reproduce the strong correlation between the TOF and the Young's moduli (Fig. 5). Based on the least square fitting of the simulation data, the TOF (in second) can be expressed mathematically as a function of Young's modulus E (in pascal):

$$\begin{aligned} TOF &= a \cdot E^b + c, \\ a &= 0.0331 \pm 0.0088 \\ b &= -0.1514 \pm 0.0228 \\ c &= -1.016 \times 10^{-4} \pm 0.313 \times 10^{-4} \end{aligned} \quad (2)$$

The coefficients are obtained with 95% confidence interval. Using this relationship, experimentally acquired TOF values were interpolated to calculate the Young's modulus of the inspected bone.

B. Cadaveric Bone Testing

Following radiographic analysis, one specimen had to be excluded from further analysis due to evident bone disease. Therefore, a total of nine specimens (n=9) were used for analysis. The analysis was focused on the proximal femur, femoral neck, greater trochanter, and inter trochanteric region.

BMD results

The specimens represented a wide range of bone quality, with proximal femur BMD measurements ranging from 0.41 g/cm² to 1.08 g/cm². The largest BMD measurements were found in the inter trochanteric region, while the smallest were found in the greater trochanter (Table 2).

Table 2

DEXA BMD Measurements.

Statistic	Proximal Femur BMD (g/cm ²)	Femoral Neck BMD (g/cm ²)	Trochanter (g/cm ²)	BMD	Inter-Trochanteric BMD (g/cm ²)
Mean	0.73	0.60	0.52		0.87
Std Dev	0.19	0.17	0.16		0.23
Median	0.68	0.51	0.47		0.85
Min	0.41	0.37	0.29		0.47
Max	1.08	0.86	0.80		1.31

Calculated Young's modulus

Calculated Young's modulus values varied depending on femoral region, as well as HNSW evaluation location (Table 3). On average, the highest strength was found in the posterior femoral neck and the anterior inter trochanteric region, with mean Young's modulus values of 0.61 GPa and 0.72 GPa, respectively. The smallest range of values was found in the femoral head, with Young's modulus values of 0.05 GPa to 0.16 GPa.

Table 3

Highly Nonlinear Solitary Wave Measurements – Calculated Young's Modulus (GPa).

Femoral Region	Location	Mean	Std Dev	Median	Min	Max
Neck	Anterior	0.30	0.16	0.31	0.11	0.55
	Posterior	0.61	0.19	0.61	0.37	0.88
	Axial	0.36	0.26	0.41	0.03	0.82
Greater Trochanter	Lateral	0.26	0.16	0.27	0.08	0.59
	Anterior	0.21	0.14	0.25	0.04	0.42
	Posterior	0.13	0.10	0.11	0.04	0.36
Inter	Anterior	0.72	0.34	0.66	0.31	1.35
	Posterior	0.19	0.16	0.17	0.01	0.54
	Axial	0.11	0.03	0.11	0.06	0.16
Head	Lateral	0.07	0.02	0.07	0.05	0.13
	Anterior	0.09	0.03	0.09	0.06	0.13
	Posterior	0.10	0.01	0.09	0.08	0.12

BMD vs. time of flight

Site-specific correlations were calculated by correlating TOF of a specific region (i.e. anterior femoral neck) with the BMD in that region (i.e. femoral neck area). High correlations were found at different locations in the proximal femur. The largest site-specific correlation was found with the posterior neck TOF correlated with femoral neck BMD, with a Pearson correlation (r) of -0.86, $p = 0.003$. The smallest site-specific correlations were from the axial greater trochanteric TOF correlated with greater trochanter BMD, and the anterior inter trochanteric TOF correlated with inter trochanteric BMD (Table 4).

Non site-specific correlations were calculated by correlating TOF of each region (i.e. anterior femoral neck) with proximal femur BMD. Non site-specific correlation values were very similar to the site-specific correlations for a given location; however, in the femoral neck and greater trochanter, the slopes of the regression lines were smaller than the site-specific regressions (Fig. 6). The site-specific slopes for the inter trochanteric region, however, were smaller than non site-specific slopes.

Table 4

Correlations of HNSW Time of Flight vs. BMD.

Femoral Region	HNSW Location	<i>Non Site-Specific</i>			<i>Site-Specific</i>		
		Pearson Correlation	P-value	Slope	Pearson Correlation	P-value	Slope
Neck	Anterior	-0.58	0.099	-0.51	-0.61	0.084	-0.61
	Posterior	-0.83	0.006	-0.27	-0.86	0.003	-0.33
	Axial	-0.50	0.170	-0.87	-0.49	0.184	-1.04
Greater Trochanter	Lateral	-0.69	0.039	-0.70	-0.77	0.016	-0.95
	Anterior	-0.82	0.007	-1.31	-0.81	0.009	-1.58
	Posterior	-0.78	0.014	-0.95	-0.76	0.017	-1.14
Inter Trochanter	Anterior	-0.84	0.004	-0.41	-0.83	0.005	-0.46
	Posterior	-0.44	0.233	-1.02	-0.43	0.244	-1.23

BMD vs. calculated Young's modulus

Site-specific correlations were calculated by correlating calculated Young's modulus (E) of a specific region (i.e. anterior femoral neck) with the BMD in that region (i.e. Femoral Neck BMD). The largest site-specific correlation was $r = 0.91$, $p = 0.001$, found for the correlation of the anterior greater trochanter Young's modulus with greater trochanter BMD. The smallest correlations were found for the anterior femoral neck Young's modulus and the anterior inter trochanteric Young's modulus (Table 5).

Table 5

Correlations of Calculated Young's Modulus vs. BMD.

Femoral Region	HNSW Location	<i>Non Site-Specific</i>			<i>Site-Specific</i>		
		Pearson Correlation	P-value	Slope	Pearson Correlation	P-value	Slope
Neck	Anterior	0.47	0.206	0.39	0.51	0.157	0.50
	Posterior	0.86	0.003	0.84	0.89	0.002	1.00
Greater Trochanter	Axial	0.79	0.011	1.07	0.78	0.013	1.30
	Lateral	0.65	0.056	0.55	0.76	0.017	0.80

	Anterior	0.91	0.001	0.66	0.91	0.001	0.82
	Posterior	0.86	0.003	0.43	0.86	0.003	0.53
Inter	Anterior	0.91	0.001	1.61	0.90	0.001	1.31
Trochanter	Posterior	0.69	0.042	0.56	0.69	0.040	0.46

Non site-specific correlations again were very similar to those of site-specific correlations; however, once again, the slopes follow a similar trend to the time of flight correlations. In the femoral neck and greater trochanter, the slopes of the regression lines were larger for site-specific correlations than non site-specific correlations (Fig 7).

IV. DISCUSSION

This study proposes a new approach to quantify bone quality using highly nonlinear solitary waves to offer nondestructive site-specific evaluation of bone mechanical properties. The sensitivity of the HNSWs to the bone material properties, as well as their robustness, makes them useful as information carriers in the nondestructive evaluation of bone. A one-dimensional granular crystal composed of tightly packed particles is assembled to form a compact sensor device to generate and propagate robust solitary waves. Via direct contact with bone specimens, this device is capable of assessing bone mechanical properties, particularly bone elasticity in this study, based on the responsiveness of the diagnostic solitary waves. The preliminary study using bone-like polyurethane foam blocks showed a close correlation between Young's modulus and the time of flight of the primary solitary waves reflected from the artificial bone interface. Exploiting the sensitive responses of HNSWs to bone mechanical properties, *in-vitro* evaluations of Young's modulus of human cadaveric femurs in highly localized regions were performed. Based on the statistical analysis, this study shows strong correlations both between site-specific BMD and derived Young's modulus measurements, as well as the non site-specific BMD and derived Young's modulus measurements, demonstrating the capability of the HNSW method to detect differences in bone density. Additionally, the slopes of the regression lines in the femoral neck and greater trochanter of site-specific correlations, two regions prone to injury, were greater than those of the regression lines for non site-specific correlations. This suggests the higher sensitivity of the HNSW method for localized measurement of bone material properties, as compared to that of the average density measurement of the proximal femur. The results suggest the potential to achieve highly localized bone quality assessment using the HNSW-based method in a noninvasive and time efficient manner.

In this study, the interaction of HNSWs with bone structures was successfully simulated using a discrete particle model that combines the granular chain and the bone structure. Based on the particle dynamics in the vicinity of granular chain and bone interface, a numerical relationship between TOF and Young's modulus of bone was derived. The numerical predictions of the Young's modulus showed excellent agreement with the experimental results as verified via the synthetic bone testing. In particular, the measured TOF showed millisecond-order responses over a range of bone rigidity variation from "high risk of fracture" and "healthy" status. This is in contrast to the microsecond transmission time change in ultrasonic wave measurements for the conventional QUS method [25]. The high responsiveness of the solitary wave enhances the reliability of solitary wave-based diagnostic method and potentially relaxes the need for expensive measurement equipments. It is also notable that the HNSW-based evaluation scheme suggests higher sensitivity in the "high risk of fracture" domain in comparison to the "healthy" domain.

The Young's modulus of cadaveric femurs has been heavily studied in the literature. For cortical bone, wide ranges of Young's modulus have been reported, with values of as low as 0.69 GPa along the femoral shaft [26], to values greater than 20 GPa [27-30]. Similarly, trabecular bone also shows a wide range, with Young's modulus values from 0.49 GPa to almost 10 GPa

[31]. The results for calculated Young's modulus also show a wide range, between 0.01 and 1.35 GPa, yet fall amongst the lower reported values. Changes in material properties occur in different regions, and depend on other confounding factors such as age, gender, bone density, and testing conditions [32-37]. While these tests measure specifically cortical or cancellous bone strength, the proposed evaluation method presents an apparent Young's modulus, represented by not only the surface of the bone (cortical shell), but possibly, the inner material as well. Therefore, it is difficult to make direct comparisons between the apparent Young's modulus values reported in this study to those reported in the literature. One previous study which took cortical bone biopsies from osteoarthritic patients showed a Young's modulus range of 0.69 GPa to 3.37 GPa, which falls much closer to the range of values reported in this study [26]. Additionally, with reported decreases in trabecular bone qualities from radiographic analysis in that study, the combined apparent range of Young's modulus would be noticeably lower.

Previous studies investigated the relationship between bone density and femoral bone strength. The literature indicates a positive correlation between Young's modulus and BMD in human cadaveric femurs [26, 32, 37-38]. However, the correlations often vary greatly for both cortical and trabecular, as well as between one another [26, 32, 37, 39-42]. These differences are largely due to anisotropic differences across the femoral region [33, 41]. The variation of bone strength along different directions and at different location within a particular region varies greatly, and thus would affect the correlation between BMD and mechanical strength. Additionally, it has been shown that cortical thinning occurs more along specific axes, and thus non-homogeneously affecting the bone quality [35-36, 43].

Due to these discrepancies, the necessity of a site-specific measurement of bone quality for fracture risk assessment is clear. In this study, high site-specific correlations in all three regions, including the femoral neck, greater trochanter, and inter trochanteric region, were found. Measurements show Pearson correlation values as high as $r = 0.91$, $p=0.001$. However, low correlations were also found in some regional measurements, such as at the anterior femoral neck (when compared to femoral neck BMD), with a correlation of $r = 0.51$. This regional difference could simply be a result of the non-site-specific scanning technique employed by DEXA. The BMD measurements may have been more heavily influenced by the posterior region, and thus, the calculated Young's modulus in the posterior femoral neck location correlates better with the femoral neck BMD than the anterior region. Additionally, the range of correlations could be due to anisotropic differences, cortical thinning, etc.

In addition to high correlations between calculated Young's modulus and BMD, the slopes of the regression lines were higher, in the femoral neck and greater trochanter, for site-specific correlations as compared to non site-specific (HNSW measurement versus proximal femur BMD). This suggests that the evaluation of bone quality is more sensitive in specific regions when correlated with specific region bone density measurements. Based on the presented high correlations and larger regression line slopes for site-specific comparisons, the proposed method shows potential to address some of the shortcomings in current technology, such as the areal scanning method used in DEXA.

As bone density is not a comprehensive measure of overall bone quality, the need for a mechanical based clinical assessment of bone quality is clear [9, 44]. Due to the anisotropic changes along various regions of the bone, specifically in the proximal femur, an average bone density (i.e. BMD by DEXA) may not provide the best predictor of hip fracture. The inconsistencies in prediction are represented by the range of correlation strengths between BMD and fracture risk. The proposed evaluation method provides a site-specific measurement of bone quality, as calculated Young's modulus values range for various regions and locations in the proximal femur. This is consistent with literature, reporting varying strength and stiffness depending on the direction and location of measurement.

In addition to the ability of the proposed evaluation method to provide site-specific assessment, the results can be processed almost instantaneously. The assessment of bone quality

is performed in a matter of seconds, compared with that of DEXA, which takes several minutes. Due to the high correlation with DEXA reported BMD, the apparent specificity and sensitivity, as well as the quick assessment time, this proposed method shows great promise as a determinant of bone quality.

This study has been limited to the evaluation of bone Young's modulus rather than the direct assessment of bone fracture risk. Moreover, for the sake of simplicity in numerical simulations, we assumed that bone material properties are approximately uniform in a localized region of inspection. Hence, further study will be needed to address the anisotropic and nonhomogeneous nature of bone and to investigate the responsiveness of HNSWs to the fracture risk of bone. The future plan also includes miniaturizing the sensor/actuator prototype to improve accessibility of entire regions of the femur to obtain multiple measurements in various locations in a given region, such as in the femoral neck. Lastly, to use this technique *in-vivo* on the surface of patients' skin (e.g., heel tip or tibia), experiments investigating the effect of soft tissue layers between the device and the bone on the formation and propagation of HNSWs must be performed.

This study establishes the foundation for utilizing highly nonlinear solitary waves in nondestructive site-specific evaluation of bone mechanical properties. We project that the HNSW-based method could potentially supplement conventional methods of determining bone quality, and prove to be useful in early and noninvasive detection of fracture risks.

Acknowledgements

The authors are very grateful to Ashleen Knutsen and Sachith Dunatunga for their assistance in preparing specimens and performing tests, as well as Jeremy Kalma for his assistance with figure illustrations in addition to the aforementioned experimental tasks.

References

1. Nixon, M., et al., *Does bone quality predict loosening of cemented total hip replacements?* J Bone Joint Surg Br, 2007. **89**(10): p. 1303-8.
2. Kurtz, S.M., et al., *Future young patient demand for primary and revision joint replacement: national projections from 2010 to 2030.* Clin Orthop Relat Res, 2009. **467**(10): p. 2606-12.
3. Kurtz, S.M., et al., *Future clinical and economic impact of revision total hip and knee arthroplasty.* J Bone Joint Surg Am, 2007. **89 Suppl 3**: p. 144-51.
4. Hernandez, C.J. and T.M. Keaveny, *A biomechanical perspective on bone quality.* Bone, 2006. **39**(6): p. 1173-81.
5. Kanis, J.A., *Diagnosis of osteoporosis and assessment of fracture risk.* Lancet, 2002. **359**(9321): p. 1929-36.
6. Lochmuller, E.M., et al., *Can novel clinical densitometric techniques replace or improve DXA in predicting bone strength in osteoporosis at the hip and other skeletal sites?* J Bone Miner Res, 2003. **18**(5): p. 906-12.
7. Stewart, A., V. Kumar, and D.M. Reid, *Long-term fracture prediction by DXA and QUS: a 10-year prospective study.* J Bone Miner Res, 2006. **21**(3): p. 413-8.
8. Myers, E.R., et al., *Geometric variables from DXA of the radius predict forearm fracture load in vitro.* Calcif Tissue Int, 1993. **52**(3): p. 199-204.
9. Roberts, B.J., et al., *Comparison of hip fracture risk prediction by femoral BMD and by the factor of risk for hip fracture derived from direct measurements of femoral strength.* Bone, 2009.
10. Nesterenko, V.F., *Dynamics of Heterogeneous Materials.* 2001, New York: Springer-Verlag New York, Inc.
11. Sen, S., et al., *Solitary waves in the granular chain.* Physics Reports, 2008. **462**(2): p. 21-66.

12. Daraio, C., et al., *Energy trapping and shock disintegration in a composite granular medium*. Physical Review Letters, 2006. **96**(5).
13. Herbold, E.B. and V.F. Nesterenko, *Shock wave structure in a strongly nonlinear lattice with viscous dissipation*. Physical Review E, 2007. **75**(2).
14. Spadoni, A. and C. Daraio, *Generation and control of sound bullets with a nonlinear acoustic lens*. Proc Natl Acad Sci U S A, 2010.
15. Khatri, D., C. Daraio, and P. Rizzo, *Coupling of Highly Nonlinear Waves with Linear Elastic Media*. Proc SPIE Int Soc Opt Eng, 2009: p. 6934-6934.
16. Daraio, C., et al., *Tunability of solitary wave properties in one-dimensional strongly nonlinear phononic crystals*. Phys Rev E Stat Nonlin Soft Matter Phys, 2006. **73**(2 Pt 2): p. 026610.
17. Job, S., et al., *How Hertzian solitary waves interact with boundaries in a 1D granular medium*. Physical Review Letters, 2005. **94**(17).
18. Yang, J., et al., *Interaction of highly nonlinear solitary waves with linear elastic media (arXiv to be added)*. Physical Review E 2010.
19. Nesterenko, V.F., et al., *Anomalous wave reflection at the interface of two strongly nonlinear granular media*. Physical Review Letters, 2005. **95**(15).
20. Shampine, L.F. and M.W. Reichelt, *The MATLAB ODE Suite*. SIAM J. Sci. Comput., 1997. **18**(1): p. 1-22.
21. <http://www.sawbones.com/products/bio/testblocks/solidfoam.aspx>.
22. Calvert, et al., *Characterization of commercial rigid polyurethane foams used as bone analogs for implant testing*. Vol. 21. 2010, Heidelberg, ALLEMAGNE: Springer. 9.
23. Hayes, W.C., S.J. Piazza, and P.K. Zysset, *Biomechanics of fracture risk prediction of the hip and spine by quantitative computed tomography*. Radiol Clin North Am, 1991. **29**(1): p. 1-18.
24. Wu, S.Y., et al., *Assessment of volumetric bone mineral density of the femoral neck in postmenopausal women with and without vertebral fractures using quantitative multi-slice CT*. J Zhejiang Univ Sci B, 2009. **10**(7): p. 499-504.
25. Baroncelli, G.I., et al., *Analysis of quantitative ultrasound graphic trace and derived variables assessed at proximal phalanges of the hand in healthy subjects and in patients with cerebral palsy or juvenile idiopathic arthritis.: A pilot study*. Bone, 2010. **46**(1): p. 182-189.
26. Wachter, N.J., et al., *Correlation of bone mineral density with strength and microstructural parameters of cortical bone in vitro*. Bone, 2002. **31**(1): p. 90-5.
27. Bayraktar, H.H., et al., *Comparison of the elastic and yield properties of human femoral trabecular and cortical bone tissue*. J Biomech, 2004. **37**(1): p. 27-35.
28. Rho, J.Y., R.B. Ashman, and C.H. Turner, *Young's modulus of trabecular and cortical bone material: ultrasonic and microtensile measurements*. J Biomech, 1993. **26**(2): p. 111-9.
29. Wirtz, D.C., et al., *Critical evaluation of known bone material properties to realize anisotropic FE-simulation of the proximal femur*. J Biomech, 2000. **33**(10): p. 1325-30.
30. Keller, T.S., Z. Mao, and D.M. Spengler, *Young's modulus, bending strength, and tissue physical properties of human compact bone*. J Orthop Res, 1990. **8**(4): p. 592-603.
31. Goldstein, S.A., *The mechanical properties of trabecular bone: dependence on anatomic location and function*. J Biomech, 1987. **20**(11-12): p. 1055-61.
32. Esses, S.I., J.C. Lotz, and W.C. Hayes, *Biomechanical properties of the proximal femur determined in vitro by single-energy quantitative computed tomography*. J Bone Miner Res, 1989. **4**(5): p. 715-22.
33. Augat, P., et al., *Anisotropy of the elastic modulus of trabecular bone specimens from different anatomical locations*. Med Eng Phys, 1998. **20**(2): p. 124-31.

34. Reilly, D.T. and A.H. Burstein, *Review article. The mechanical properties of cortical bone.* J Bone Joint Surg Am, 1974. **56**(5): p. 1001-22.
35. Crofts, R.D., T.M. Boyce, and R.D. Bloebaum, *Aging changes in osteon mineralization in the human femoral neck.* Bone, 1994. **15**(2): p. 147-52.
36. Bell, K.L., et al., *Regional differences in cortical porosity in the fractured femoral neck.* Bone, 1999. **24**(1): p. 57-64.
37. Majumdar, S., et al., *High-resolution magnetic resonance imaging: three-dimensional trabecular bone architecture and biomechanical properties.* Bone, 1998. **22**(5): p. 445-54.
38. Snyder, S.M. and E. Schneider, *Estimation of mechanical properties of cortical bone by computed tomography.* J Orthop Res, 1991. **9**(3): p. 422-31.
39. Schoenfeld, C.M., E.P. Lautenschlager, and P.R. Meyer, Jr., *Mechanical properties of human cancellous bone in the femoral head.* Med Biol Eng, 1974. **12**(3): p. 313-7.
40. Majumdar, S., et al., *Fractal analysis of radiographs: assessment of trabecular bone structure and prediction of elastic modulus and strength.* Med Phys, 1999. **26**(7): p. 1330-40.
41. Zhu, M., et al., *Multiplanar variations in the structural characteristics of cancellous bone.* Bone, 1994. **15**(3): p. 251-9.
42. Ciarelli, M.J., et al., *Evaluation of orthogonal mechanical properties and density of human trabecular bone from the major metaphyseal regions with materials testing and computed tomography.* J Orthop Res, 1991. **9**(5): p. 674-82.
43. Bell, K.L., et al., *Structure of the femoral neck in hip fracture: cortical bone loss in the inferoanterior to superoposterior axis.* J Bone Miner Res, 1999. **14**(1): p. 111-9.
44. Wynnyckyj, C., et al., *A new tool to assess the mechanical properties of bone due to collagen degradation.* Bone, 2009. **44**(5): p. 840-8.

Figure 1. (Color online) Schematic diagram of a granular crystal-based sensor. The vertical chain is composed of 20 spherical particles constrained by guides. The incident and reflected HNSWs, triggered by the striker impact, are recorded by the instrumented bead.

Figure 2. A one-dimensional granular chain of spherical elements in contact with bone structure (top). The interaction of granular particles with the bounding bone can be modeled using a discrete particle model composed of point masses and nonlinear springs (bottom).

Figure 3. Schematic diagram of human femur with 12 measurement locations for solitary wave-based evaluation in anterior (left) and posterior (right) views.

Figure 4. (Color online) Solitary wave interaction with artificial bone samples. The blue lines denote numerical force profiles, while the green lines represent experimental measurements. The signals are shifted by 100N apart. A group of rigid polyurethane foam simulates clinical bone quality ranging from healthy to osteoporotic status. The time-of-flight (TOF) values are extracted from the raw signals by measuring the time elapsed between the incident and the first reflected waves, measured at the sensor-implemented bead.

Figure 5. Time of flight values as a function of elastic moduli. The blue line denotes the numerical results based on the discrete particle model, while the circles represent the experimental results. The error bars are standard deviation values obtained from five experimental measurements using artificial bone specimens. The “high risk of fracture” or “osteoporotic” samples generate larger TOF values in comparison to the “healthy” specimens.

Figure 6. Correlations for time of flight versus BMD. (a) Non site-specific, femoral neck TOF (time of flight) versus proximal femur BMD. (b) Non site-specific, greater trochanter TOF versus proximal femur BMD. (c) Non site-specific, inter trochanteric TOF versus proximal femur BMD. (d) Site-specific, femoral neck TOF versus femoral neck BMD. (e) Site-specific, greater trochanter TOF versus greater trochanter BMD. (f) Site-specific, inter trochanteric TOF versus inter trochanteric BMD.

Figure 7. Correlations for calculated Young’s modulus versus BMD. (a) Non site-specific, femoral neck Young’s modulus versus proximal femur BMD. (b) Non site-specific, greater trochanter Young’s modulus versus proximal femur BMD. (c) Non site-specific, inter trochanteric Young’s modulus versus proximal femur BMD. (d) Site-specific, femoral neck Young’s modulus versus femoral neck BMD. (e) Site-specific, greater trochanter Young’s modulus versus greater trochanter BMD. (f) Site-specific, inter trochanteric Young’s modulus versus inter trochanteric BMD.

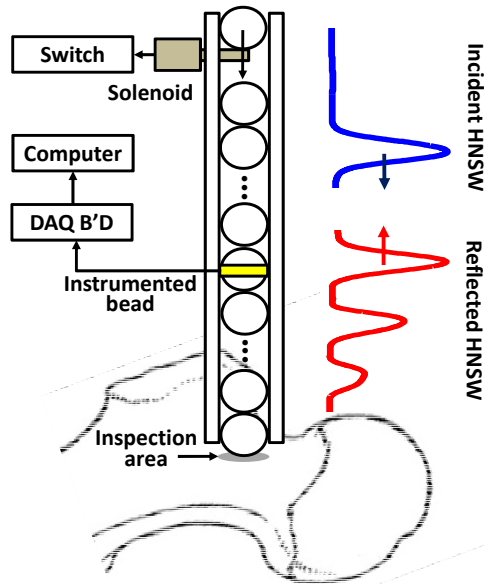


FIGURE 1

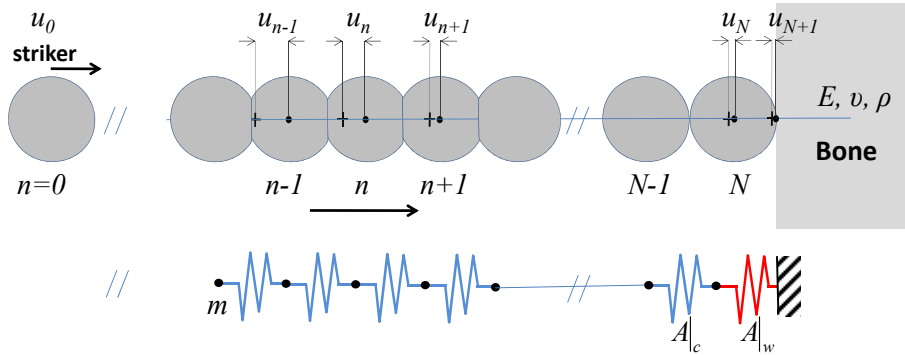


FIGURE 2

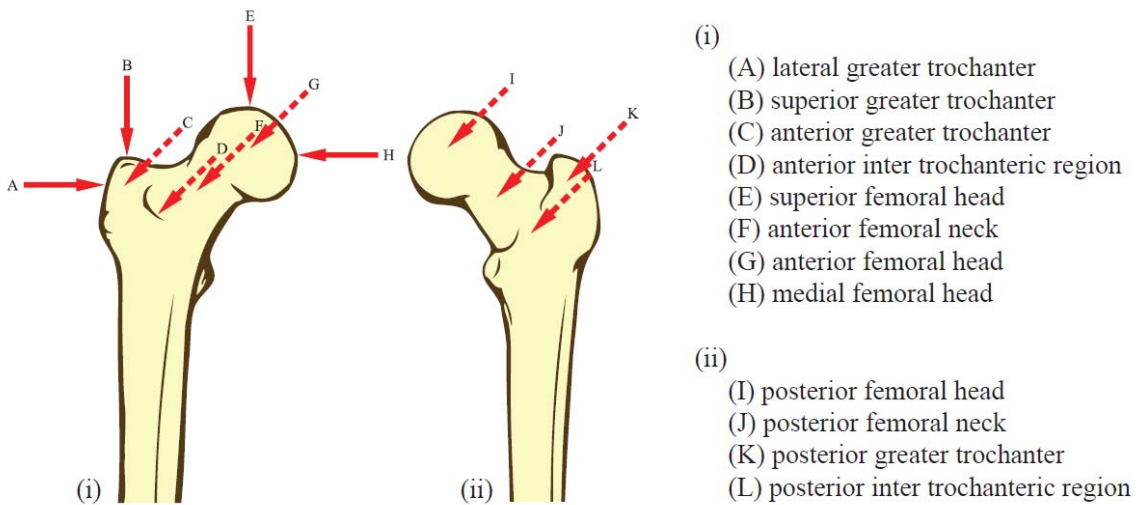


FIGURE 3

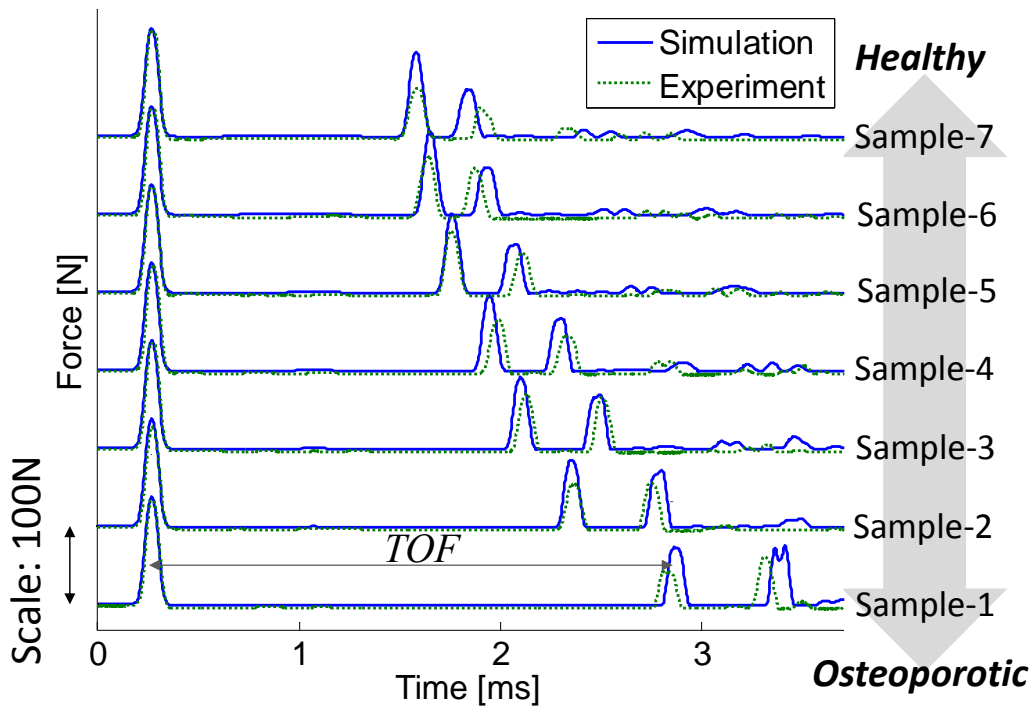


FIGURE 4

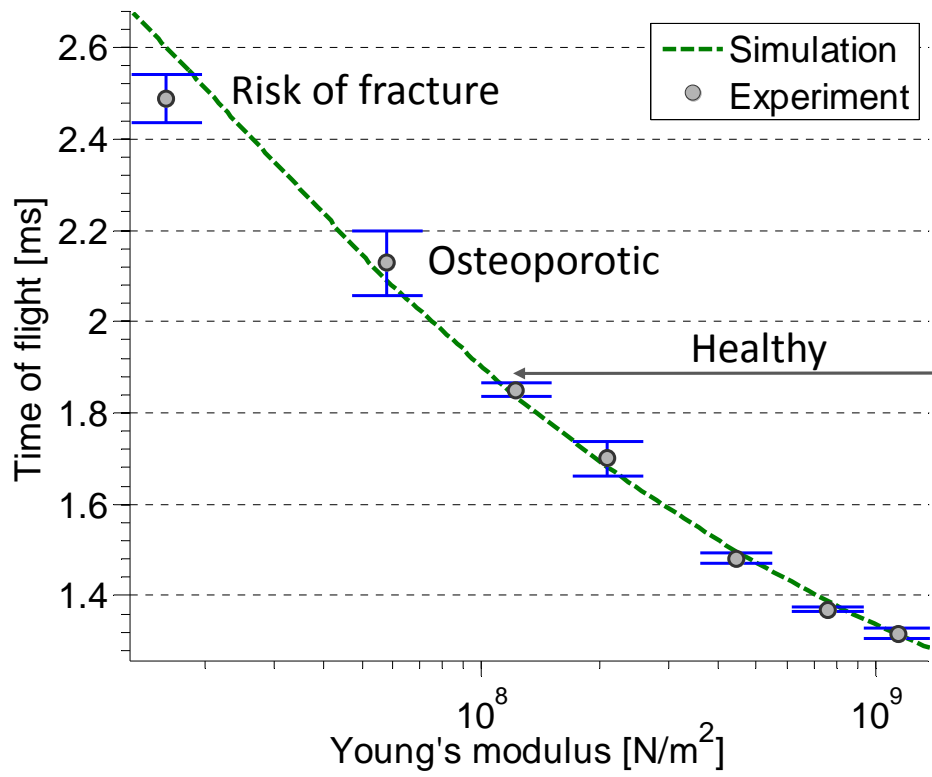


FIGURE 5

